時差環境下における視交叉上核分子神経シグナルに関する研究

2014

鈴木　暢

Molecular and neuronal signaling in the SCN for the regulation of reentrainment during jet lag

2014

Toru Suzuki

Contents

Preface……3

Chapter 1:
Mice genetically deficient in vasopressin V1a and V1b receptors are resistant to jet lag……4

Introduction……..…….……5
Results…….……...……7
Discussion……..…….....26

Chapter 2:
Behavioral difference in mice after two ways of jet lag:
light-phase advance and dark-phase advance……28

Materials and Methods……..29

References……33

Acknowledgments……...…….……...……38

Preface

Animals including human beings have an internal clock oscillating every 24 hrs. This circadian clock controls the daily rhythms in many physiological phenomena such as activity/rest cycles, body temperature, and hormone secretion, which enables us to anticipate the proper timing for better outcome. Nowadays, however, the circadian system can be disrupted by social or personal reasons. Jet lag is one of the most interesting cause for this failure. When we go abroad, jet-lag symptoms arise from temporal misalignment between the internal circadian clock and external solar time, causing sleep disturbances and gastrointestinal distress. In addition, evidence has accumulated that repeated jet-lag exposure in flight attendants or shift works can be a risk factor for health problems such as cancers, cardiovascular diseases, and type 2 diabetes. However, little is known about the molecular and neuronal mechanisms which regulate jet lag.

In Chapter 1, I show that circadian rhythms of behavior (locomotor activity), clock gene expression, and body temperature immediately reentrained to phase-shifted light-dark cycles in mice lacking vasopressin receptors V1a and V1b (*V1a*$^{-/-}$*V1b*$^{-/-}$ mice). Nevertheless, the behavior of *V1a*$^{-/-}$*V1b*$^{-/-}$ mice was still coupled to the internal clock, which oscillated normally under standard conditions. Experiments with suprachiasmatic nucleus (SCN) slices in culture suggested that interneuronal communication mediated by V1a and V1b confers on the SCN an intrinsic resistance to external perturbation. Pharmacological blockade of V1a and V1b in the SCN of wild-type mice resulted in accelerated recovery from jet lag which highlights the potential of vasopressin signaling as a therapeutic target for management of circadian rhythm misalignment, such as jet lag and shift work.

There are two ways of 8-hr phase advances in LD cycles, experimentally: new LD cycles abruptly start at ZT16 which is in dark phase before jet lag or abruptly start at ZT4 which is in light phase before jet lag. In Chapter 2, I examine the differential regulation of the amounts of phase shifts of locomotor activities between two ways of jet lag conditions.

Chapter 1

Mice genetically deficient in vasopressin V1a and V1b receptors are resistant to jet lag.

Introduction

The endogenous circadian clock drives oscillations in physiology and behavior with a period of about 24 hrs. We are not usually aware of this system because it is completely synchronized with environmental light-dark cycles, but travelling rapidly across multiple time zones suddenly makes us aware of the desynchrony, causing sleep disturbances and gastrointestinal distress (Comperatore and Krueger 1990; Sack 2009). Repeated jet-lag exposure and rotating shift work increase the risk of lifestyle-related diseases, such as cardiovascular complaints and metabolic insufficiency (Buxton et al. 2012; Scheer et al. 2009). Although jet lag is recognized as a chronobiological problem (Kiessling et al. 2010; Yamazaki et al. 2000; Reddy et al. 2002), specific molecular and cellular mechanisms underlying jet lag are poorly understood.

In mammals, internal time is orchestrated by the master clock in the hypothalamic suprachiasmatic nucleus (SCN), whose coherent output signal synchronizes cell clocks throughout the body (Yamaguchi et al. 2003; Mohawk and Takahashi 2011; Aton et al. 2005; Butler and Silver 2009; Maywood et al. 2011; Cao et al. 2013). The SCN is anatomically and functionally organized into two subdivisions, the ventrolateral region and the dorsomedial region. The ventrolateral region that lies above the optic chiasm comprises mainly neurons producing vasoactive intestinal polypeptide (VIP). The dorsomedial region contains a large population of arginine vasopressin (AVP)-producing neurons. AVP is indeed expressed in about 40% neurons of the SCN (Moore et al. 2002). Almost all cells have circadian clocks. Those clocks have been proposed as consisting of autoregulatory loops in which transcriptional feedback and regulated protein turnover are used to maintain a 24-hr periodicity. That mechanism is explained by effects of transcriptional activators and repressors that constitute negative feedback loops (Reppert and Weaver 2002; Hastings et al. 2008; Liu et al. 2007) The transcriptional activators CLOCK and BMAL1 form heterodimers and activate transcription of *Period* (*Per1* and *Per2*) and *Cryptochrome* (*Cry1* and *Cry2*) genes by binding to E-box elements present in their promoters. Once the repressor proteins, PER and CRY, reach critical concentrations, they form heterodimers and inhibit their own expression by repressing the CLOCK/BMAL1 complexes.

A misalignment of SCN clock signals and environmental time cues (e.g., light and temperature) would occur during jet lag. To identify candidate signaling molecules that might contribute to jet lag, our research group designed a screening strategy (Okamura 2007), in which we (i) used histochemistry to identify genes whose expression is enriched in the mouse SCN, (ii) generated mutant mice lacking candidate genes of interest, and

(iii) measured the locomotor activity of the mutant mice under experimental jet-lag conditions. Genes encoding brain peptides and their receptors were the initial candidates of interest, because many of them are expressed in the SCN (van den Pol and Tsujimoto 1985). Our group identified arginine vasopressin (AVP) and its receptors (V1a and V1b receptors) as strong candidates. The circadian expression pattern of these proteins has been studied (Schwartz and Reppert 1985; Swaab et al. 1975; Young et al. 1993), but their roles in the circadian clock are unclear, with the exception of the V1a receptor. Genetic deletion of this receptor causes period elongation in mice (Li et al. 2009).

Results

Locomotor activities during jet lag.

I generated V1a and V1b receptor double knockout mice (*V1a*$^{-/-}$*V1b*$^{-/-}$ mice) (Koshimizu et al. 2006; Tanoue et al. 2004; see Materials and Methods) and examined their behavioral rhythms under experimental jet-lag conditions. The mice were housed in a light (~200 lux)–controlled isolator with food and drink ad libitum, and their spontaneous locomotor activity was recorded by infrared sensor (Fig. 1) or voluntary wheel running (Fig. 2).

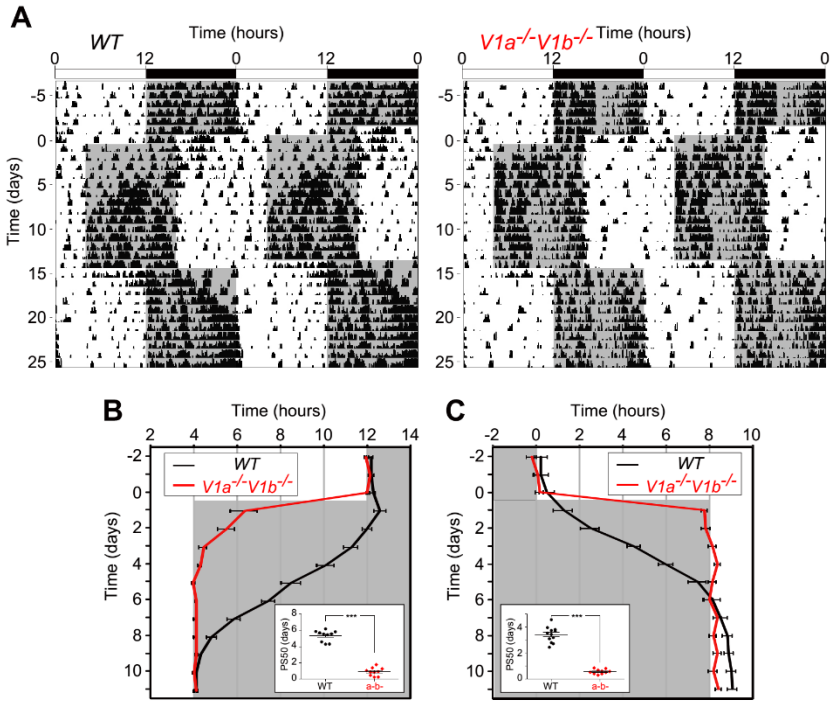

Fig. 1. *V1a*$^{-/-}$*V1b*$^{-/-}$ mice subjected to an experimental jet-lag paradigm show immediate reentrainment to a new light-dark cycle. (A) Representative double-plotted actograms of WT (left) and *V1a*$^{-/-}$*V1b*$^{-/-}$ (right) mice subjected to an 8-hr phase advance and delay in LD cycles. (B) Activity onset in the 8-hr phase advance [means ± SEM; n = 10 (both genotypes)]. (C) Activity offset in 8-hr phase delay [means ± SEM; n = 12 (WT) and 10 (*V1a*$^{-/-}$*V1b*$^{-/-}$)]. Insets (B and C) indicate PS50 values in phase advance and in phase delay (means ± SEM; ***$P < 0.001$, unpaired *t* test). For this and subsequent figures, white and gray background indicates lights on and off, respectively. Black and red colors indicate WT and *V1a*$^{-/-}$*V1b*$^{-/-}$, respectively. Top bars indicate the initial LD cycle.

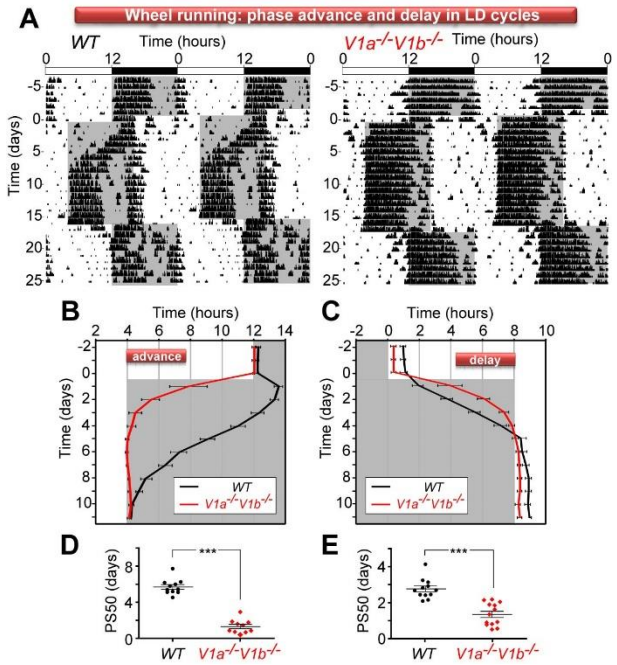

Fig. 2. Immediate reentrainment in behavioral rhythm to a new light-dark cycle in *V1a*$^{-/-}$*V1b*$^{-/-}$ mice under experimental jet lag paradigm detected by voluntary wheel running. (A) Representative double-plotted actograms of WT (left) and *V1a*$^{-/-}$*V1b*$^{-/-}$ (right) mice subjected to 8-hr phase advance (day 1) and delay (day 17) in LD cycles. Top bars indicate initial LD cycle. (B) Activity onset in 8-hr phase advance (means ± SEM; n = 11 (WT) and 10 (*V1a*$^{-/-}$*V1b*$^{-/-}$)). (C) Activity offset in 8-hr phase delay (means ± SEM; n = 12 (WT) and 13 (*V1a*$^{-/-}$*V1b*$^{-/-}$). (D and E) PS50 values of phase advance and phase delay (means ± SEM; ***$P < 0.001$, unpaired *t* test). Black and red colors indicate *WT* and *V1a*$^{-/-}$*V1b*$^{-/-}$, respectively.

When they were maintained in a 12-hr light/12-hr dark (LD) cycle, both wild-type (WT) and *V1a*$^{-/-}$*V1b*$^{-/-}$ mice exhibited high locomotor activity during the dark phase. After 2 weeks of behavior recording, LD cycles were advanced by 8 hrs. In WT mice, this advance evoked a gradual shift of locomotor activity rhythms, which took 8 to 10 days for complete reentrainment to the new LD schedule (Fig. 1, A and B). This slow resetting of locomotor activity rhythm—which is characterized by an activity onset that is not synchronous with "lights off" as normally observed, but is delayed into the night—was expected, as it is the typical sign that mice are experiencing jet lag. Every subsequent day after the LD cycle advance, the WT mice will start their activity slightly earlier, to finally align, after 8 to 10 days, to the beginning of the night. In contrast, *V1a*$^{-/-}$*V1b*$^{-/-}$ mice showed almost immediate reentrainment with only 2 to 4 days of transition (Fig. 1A).

For quantitative comparison between genotypes, I calculated the 50% phase-shift value (PS50) (Kiessling et al. 2010) and found that *V1a*$^{-/-}$*V1b*$^{-/-}$ mice reentrained more rapidly than WT mice (Fig. 1B, inset) ($P < 0.001$, unpaired *t* test). When the LD cycles were then

delayed by 8 hrs (Fig. 1, A and C) and found that, although WT mice required 5 to 6 days for reentrainment, *V1a*$^{-/-}$*V1b*$^{-/-}$ mice required only 1 day (Fig.1, A and C), and PS50 was also much smaller in *V1a*$^{-/-}$*V1b*$^{-/-}$ mice (Fig. 1C, inset) ($P < 0.001$, unpaired t test). I next examined which AVP receptor, V1a or V1b, dictates the rate of reentrainment after phase shift and found that single knockout (*V1a*$^{-/-}$*V1b*$^{+/+}$ mice and *V1a*$^{+/+}$*V1b*$^{-/-}$) mice showed intermediate rates of reentrainment (Figs. 3 and 4), which indicated that both receptors contribute to the accelerated reentrainment after jet lag.

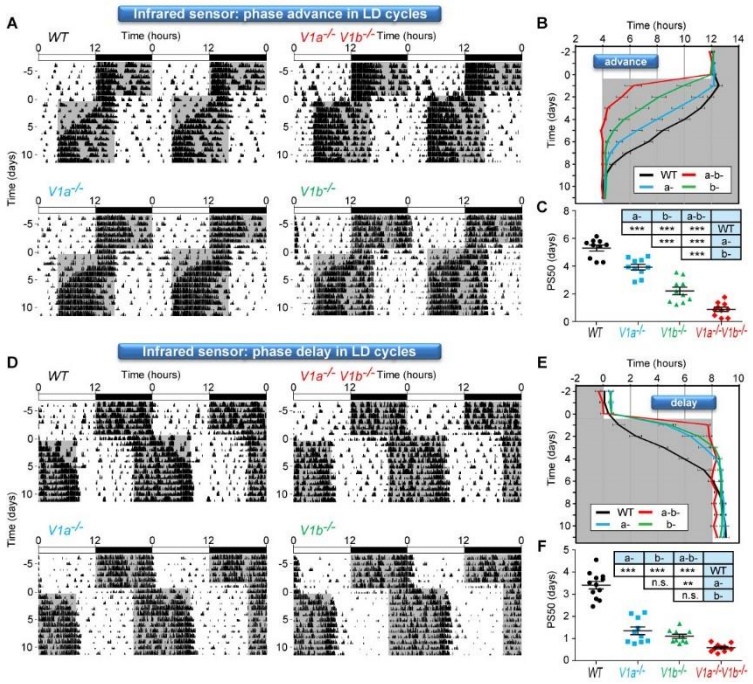

Fig. 3. Effect of jet lag task on locomotor activity rhythms in WT, *V1a*$^{-/-}$*V1b*$^{+/+}$, *V1a*$^{+/+}$*V1b*$^{-/-}$, and *V1a*$^{-/-}$*V1b*$^{-/-}$ mice detected by infrared sensor. (A) Representative double-plotted actograms of mice (WT: upper left, *V1a*$^{-/-}$*V1b*$^{+/+}$: lower left, *V1a*$^{+/+}$*V1b*$^{-/-}$: lower right, *V1a*$^{-/-}$*V1b*$^{-/-}$: upper right) subjected to 8-hr phase advance in LD cycles. (B) Activity onset in 8-hr phase advance (means ± SEM; n = 10 for all genotypes). (C) PS50 values in 8-hr phase advance (means ± SEM). One-way ANOVA, $F(3, 36) = 81.65$, $P < 0.0001$. (D) Representative double-plotted actograms of mice (as in panel A) subjected to 8-hr phase delay (E) Activity offset in 8-hr phase delay (means ± SEM; n = 12 (WT) and 10 (*V1a*$^{-/-}$*V1b*$^{+/+}$, *V1a*$^{+/+}$*V1b*$^{-/-}$, and *V1a*$^{-/-}$*V1b*$^{-/-}$). (F) PS50 values in 8-hr phase delay (means ± SEM). One-way ANOVA, $F(3, 38) = 86.02$, $P < 0.0001$. Tukey-Kramer post-hoc test was performed for comparison among the groups. *, **, and ***P indicate less than 0.05, 0.01, and 0.001, respectively. Top bars indicate initial LD cycle. Black, blue, green, and red colors indicate WT, *V1a*$^{-/-}$*V1b*$^{+/+}$, *V1a*$^{+/+}$*V1b*$^{-/-}$, and *V1a*$^{-/-}$*V1b*$^{-/-}$, respectively. The data of WT and *V1a*$^{-/-}$*V1b*$^{-/-}$ mice are identical to those shown in Fig. 1

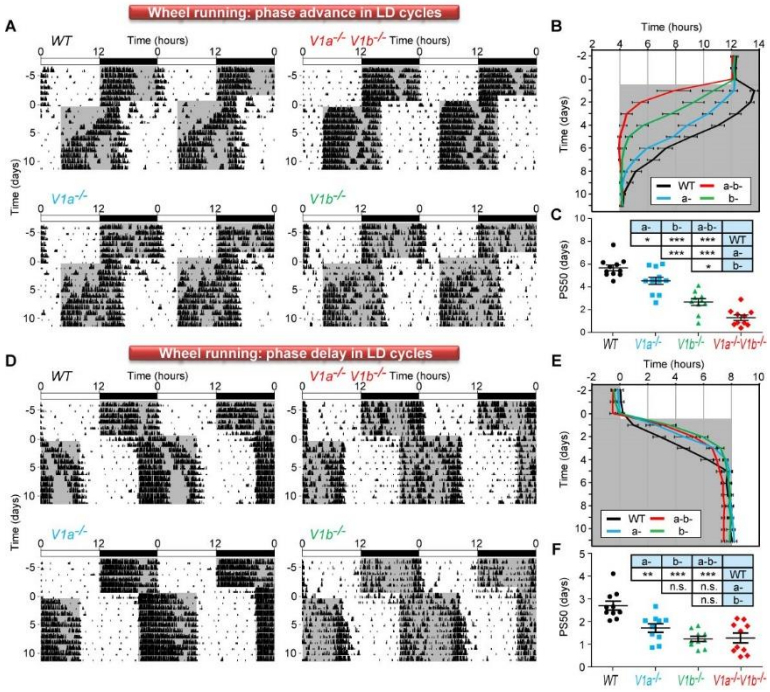

Fig. 4. Effect of jet lag task on locomotor activity rhythms in WT, *V1a*$^{-/-}$*V1b*$^{+/+}$, *V1a*$^{+/+}$*V1b*$^{-/-}$, and *V1a*$^{-/-}$*V1b*$^{-/-}$ mice detected by wheel running. (A) Representative double-plotted actograms of mice (WT: upper left, *V1a*$^{-/-}$*V1b*$^{+/+}$: lower left, *V1a*$^{+/+}$*V1b*$^{-/-}$: lower right, *V1a*$^{-/-}$*V1b*$^{-/-}$: upper right) subjected to 8-hr phase advance in LD cycles. (B) Activity onset in 8-hr phase advance (means ± SEM; n = 11 (WT), 12 (*V1a*$^{-/-}$*V1b*$^{+/+}$), and 10 (*V1a*$^{+/+}$*V1b*$^{-/-}$ and *V1a*$^{-/-}$*V1b*$^{-/-}$)). (C) PS50 values in 8-hr phase advance (means ± SEM). One-way ANOVA, F(3, 39) = 46.38, $P < 0.0001$. (D) Representative double-plotted actograms of mice (as in panel A) subjected to 8-hr phase delay (E) Activity offset in 8-hr phase delay (means ± SEM; n = 12 (WT and *V1a*$^{-/-}$*V1b*$^{+/+}$), 10 (*V1a*$^{+/+}$*V1b*$^{-/-}$), and 13 (*V1a*$^{-/-}$*V1b*$^{-/-}$)). (F) PS50 values in 8-hr phase delay (means ± SEM). One-way ANOVA, F(3, 43) = 18.62, $P < 0.0001$. Tukey-Kramer post-hoc test was performed for comparison among the groups. *, **, and ***P indicate less than 0.05, 0.01, and 0.001, respectively. Top bars indicate initial LD cycle. Black, blue, green, and red colors indicate WT, *V1a*$^{-/-}$*V1b*$^{+/+}$, *V1a*$^{+/+}$*V1b*$^{-/-}$, and *V1a*$^{-/-}$*V1b*$^{-/-}$, respectively.

Light has a dominant influence on the behavior of mice because they are nocturnal animals; it inhibits their locomotor activity or foraging behavior. To exclude the possibility that the locomotor activity of *V1a*$^{-/-}$*V1b*$^{-/-}$ mice is merely caused by the ambient LD cycle, I released mice in constant darkness (DD) after a transient advance in LD cycles. After 4, 3, 2, and only 1 day advance in the LD cycle, larger phase advances in the free-running behavior of V1a$^{-/-}$V1b$^{-/-}$ mice were observed compared with WT mice (Fig. 5). *V1a*$^{-/-}$*V1b*$^{-/-}$ mice also showed larger phase delays in behavior after only 1 day's delay in LD cycles (Fig. 6).

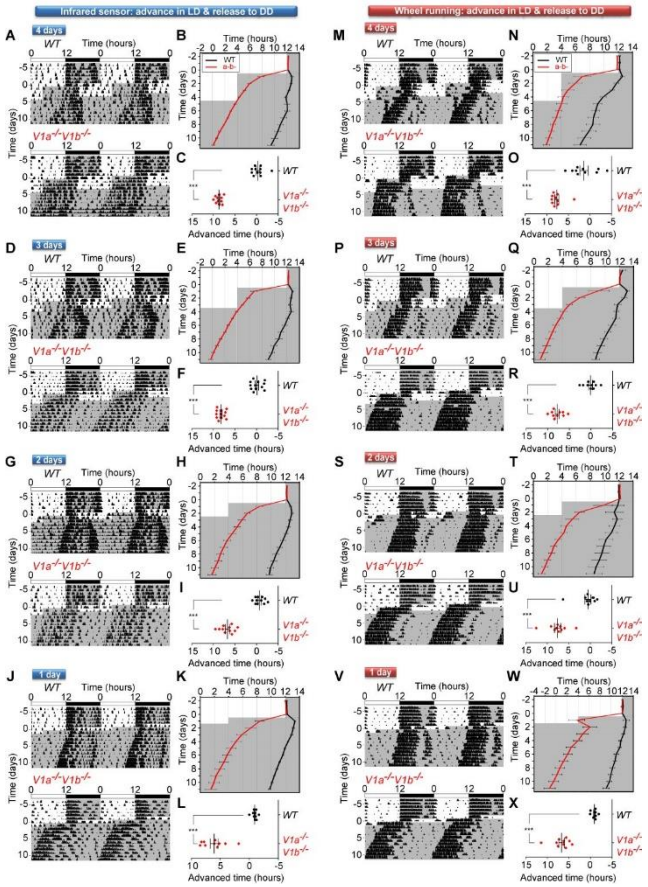

Fig. 5. Effect of transient phase advance in LD cycles on biological clock detected by infrared sensor (left: A to L) or wheel running (right: M to X). I advanced LD cycles by 8 hrs transiently for 4, 3, 2 or 1 day(s) and turned off the light. Representative double-plotted actograms of WT (upper) and *V1a*$^{-/-}$*V1b*$^{-/-}$ (lower), activity onset (means ± SEM), and amounts of phase advance values (means ± SEM) are shown as indicated in the figure (n = 10–12 for both genotypes; ***P < 0.001, unpaired t test). Note that one-day phase advance in LD cycle induces almost 8-hr advance in *V1a*$^{-/-}$*V1b*$^{-/-}$ mice behavior. Black and red colors indicate WT and *V1a*$^{-/-}$*V1b*$^{-/-}$, respectively. Top bars indicate the initial LD cycle.

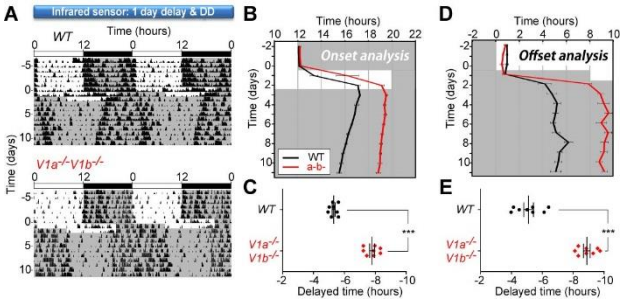

Fig. 6. Effect of one-day 8-hr phase delay in LD cycle on biological clock in WT and *V1a*$^{-/-}$*V1b*$^{-/-}$ mice detected by infrared sensor. Note that masking effect was no longer an issue in this experimental paradigm, activity onset was also used to determine the magnitude of phase delays in locomotor activity rhythm. (A) Representative double-plotted actograms of WT (upper) and *V1a*$^{-/-}$*V1b*$^{-/-}$ (lower) mice. (B) Activity onset before and after one-day 8-hr phase delay (means ± SEM; n = 8 for both genotypes). (C) Amounts of phase delay values (means ± SEM; ***P < 0.001, unpaired t test). (D) Activity offset before and after one-day 8-hr phase delay (means ± SEM; n = 8 for both genotypes). (E) Amounts of phase delay values (means ± SEM; ***P < 0.001, unpaired t test). Black and red colors indicate WT and *V1a*$^{-/-}$ *V1b*$^{-/-}$, respectively. Top bars indicate the initial LD cycle.

These findings strongly suggest that the immediate adaptation to a new LD cycle in *V1a*$^{-/-}$*V1b*$^{-/-}$ mice is not a masking effect of the environmental LD cycle but a rapid phase shift of the endogenous clock. Of note, period length under DD conditions, phase angle from LD to DD, phase response curve obtained with a short light exposure, and expression of canonical clock genes (*Per1*, *Per2*, *Bmal1*, and *Dbp*) in *V1a*$^{-/-}$*V1b*$^{-/-}$ SCN were virtually identical to those in WT mice (Figs. 7 to 9).

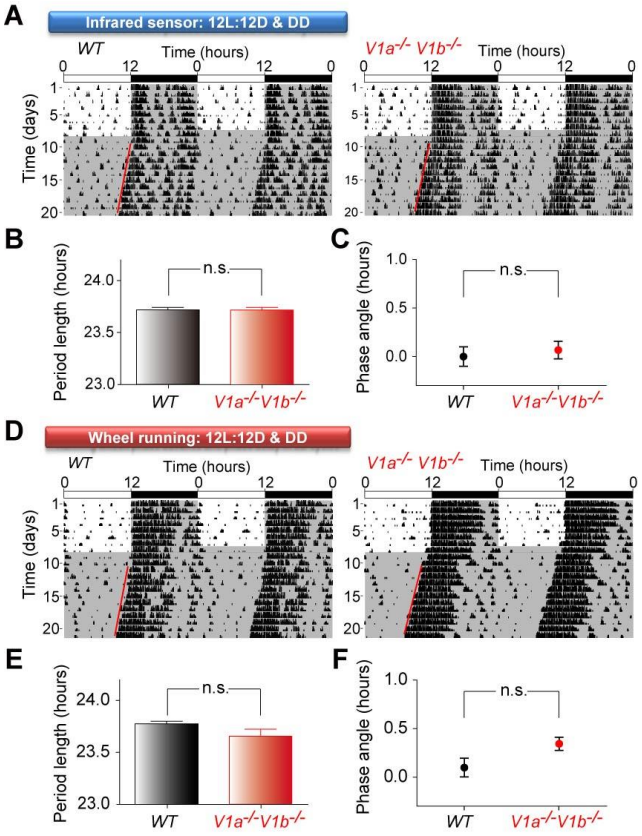

Fig. 7. Normal period length and phase angle in *V1a*$^{-/-}$*V1b*$^{-/-}$ mice detected by infrared sensor (A to C) or wheel running (D to F). (A) Representative double-plotted actograms of WT (left) and *V1a*$^{-/-}$*V1b*$^{-/-}$ (right) mice detected by infrared sensor. The red lines delineate the phase of activity onset in DD. (B) Period length of WT and *V1a*$^{-/-}$*V1b*$^{-/-}$ mice (means ± SEM; n = 10 for both genotypes). The data are identical to those shown in Fig. 1. (C) Phase angle of WT and *V1a*$^{-/-}$*V1b*$^{-/-}$ mice (means ± SEM; n = 10 for both genotypes). (D to F) Same analyses as in panels A to C were performed with wheel running (means ± SEM; n = 11 for both genotypes). Top bars indicate the initial LD cycle.

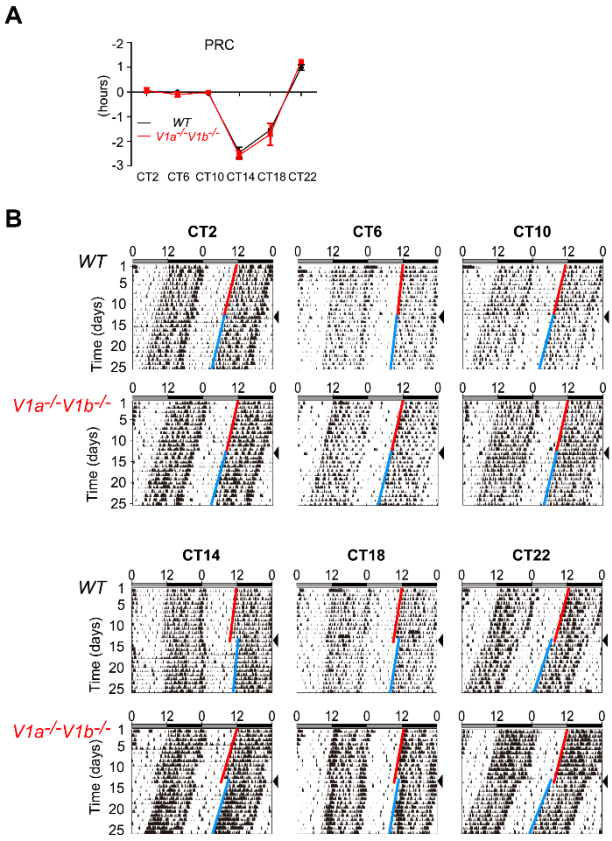

Fig. 8. Quantification of the magnitude of phase shifts by a brief light exposure (A) (n = 8 for both genotypes) and representative double-plotted actograms in each time point (B). By convention, delays are negative and advances are positive. Note that WT and *V1a*$^{-/-}$*V1b*$^{-/-}$ mice have virtually the same phase-shift magnitude at all time points. Mice were housed in DD at least for two weeks and a brief light pulse (~200 lux fluorescent light for 30 min) was given at CT2, CT6, CT10, CT14, CT18, or CT22 on the day indicated by arrowheads. Black and red colors indicate WT and *V1a*$^{-/-}$*V1b*$^{-/-}$, respectively. Top bars indicate the initial LD cycle. Red and blue lines delineate the phase of activity onset before and after a light pulse, respectively.

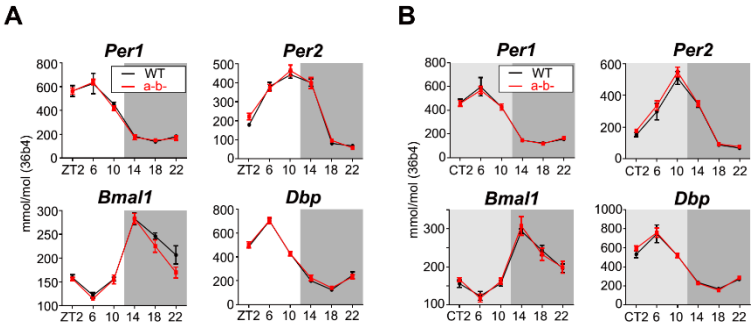

Fig. 9. Clock gene expression in the SCN under LD (A) and DD (B) conditions. SCN was dissected out by laser microdissection (see Fig. 14), and each transcript was measured by quantitative reverse transcription polymerase chain reaction (qRT-PCR) [means ± SEM; n = 5 (both genotypes in both LD and DD)]. Black and red colors indicate WT and *V1a*$^{-/-}$*V1b*$^{-/-}$, respectively.

These behavioral and molecular data exclude the possibility that rapid reentrainment in *V1a*$^{-/-}$*V1b*$^{-/-}$ mice is simply caused by a disabled clock. When behavioral experiments were performed under conditions of intermediate light intensity (~50 lux), *V1a*$^{-/-}$*V1b*$^{-/-}$ mice were found to be reentrained faster after a phase advance or phase delay (Figs. 10 and 11) and showed larger phase advances after a 1- to 4-day advance in LD cycles (Fig. 12).

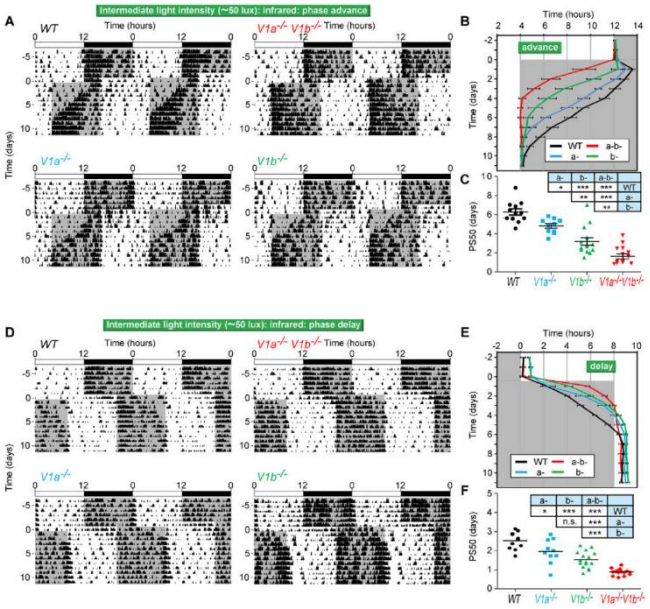

Fig. 10. Jet lag tasks under Intermediate light intensity (~50 lux). Locomotor activity rhythms were recorded by infrared sensor in WT, *V1a*$^{-/-}$*V1b*$^{+/+}$, *V1a*$^{+/+}$*V1b*$^{-/-}$, and *V1a*$^{-/-}$*V1b*$^{-/-}$ mice. (A) Representative double-plotted actograms of mice (WT: upper left, *V1a*$^{-/-}$*V1b*$^{+/+}$: lower left, *V1a*$^{+/+}$*V1b*$^{-/-}$: lower right, *V1a*$^{-/-}$*V1b*$^{-/-}$: upper right) subjected to 8-hr phase advance in LD cycles. (B) Activity onset in 8-hr phase advance (means ± SEM; n = 12 (WT), 10 (*V1a*$^{-/-}$*V1b*$^{+/+}$), 14 (*V1a*$^{+/+}$*V1b*$^{-/-}$), and 15 (*V1a*$^{-/-}$*V1b*$^{-/-}$)). (C) PS50 values in 8-hr phase advance (means ± SEM). One-way ANOVA, $F(3, 47) = 40.63$, $P < 0.0001$. (D) Representative double-plotted actograms of mice (as in panel A) subjected to 8-hr phase delay (E) Activity offset in 8-hr phase delay (means ± SEM; n = 11 (WT), 10 (*V1a*$^{-/-}$*V1b*$^{+/+}$), 16 (*V1a*$^{+/+}$*V1b*$^{-/-}$), and 15 (*V1a*$^{-/-}$*V1b*$^{-/-}$)). (F) PS50 values in 8-hr phase delay (means ± SEM). One-way ANOVA, $F(3, 48) = 32.64$, $P < 0.0001$. Tukey-Kramer post-hoc test was performed for comparison among the groups. *, **, and ***P indicate less than 0.05, 0.01, and 0.001, respectively. Top bars indicate initial LD cycle. Black, blue, green, and red colors indicate WT, *V1a*$^{-/-}$*V1b*$^{+/+}$, *V1a*$^{+/+}$*V1b*$^{-/-}$, and *V1a*$^{-/-}$*V1b*$^{-/-}$, respectively.

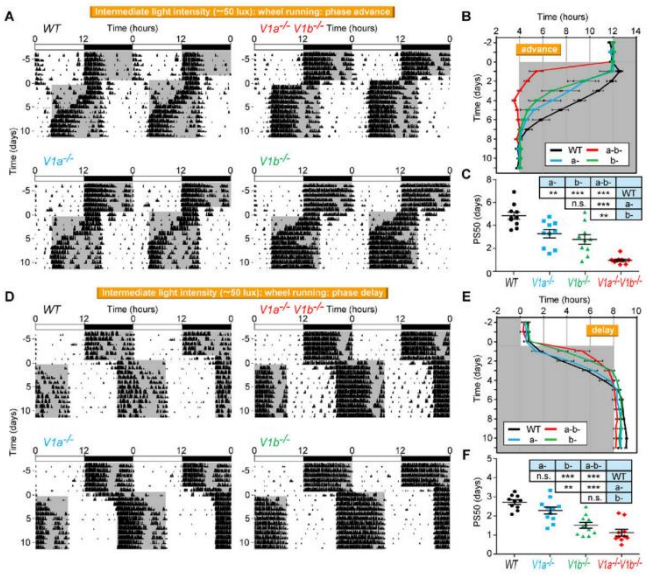

Fig. 11. Jet lag tasks under intermediate light intensity (~50 lux). Locomotor activity was recorded by wheel running in WT, *V1a*$^{-/-}$*V1b*$^{+/+}$, *V1a*$^{+/+}$*V1b*$^{-/-}$, and *V1a*$^{-/-}$*V1b*$^{-/-}$ mice. (A) Representative double-plotted actograms of mice (WT: upper left, *V1a*$^{-/-}$*V1b*$^{+/+}$: lower left, *V1a*$^{+/+}$*V1b*$^{-/-}$: lower right, *V1a*$^{-/-}$*V1b*$^{-/-}$: upper right) subjected to 8-hr phase advance in LD cycles. (B) Activity onset in 8-hr phase advance (means ± SEM; n = 10 for all genotypes). (C) PS50 values in 8-hr phase advance (means ± SEM). One-way ANOVA, F(3, 36) = 24.49, $P < 0.0001$. (D) Representative double-plotted actograms of mice (as in panel A) subjected to 8-hr phase delay (E) Activity offset in 8-hr phase delay (means ± SEM; n = 10 (WT and *V1a*$^{-/-}$*V1b*$^{-/-}$) and 11 (*V1a*$^{-/-}$*V1b*$^{+/+}$ and *V1a*$^{+/+}$*V1b*$^{-/-}$)). (F) PS50 values in 8-hr phase delay (means ± SEM). One-way ANOVA, F(3, 38) = 20.11, $P < 0.0001$. Tukey-Kramer post-hoc test was performed for comparison among the groups. ** and ***P indicate less than 0.01 and 0.001, respectively. Top bars indicate initial LD cycle. Black, blue, green, and red colors indicate WT, *V1a*$^{-/-}$*V1b*$^{+/+}$, *V1a*$^{+/+}$*V1b*$^{-/-}$, and *V1a*$^{-/-}$*V1b*$^{-/-}$, respectively.

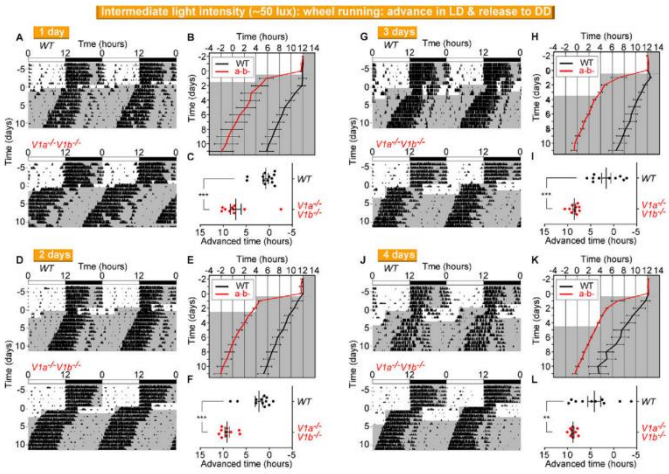

Fig. 12. Effect of transient phase advance in LD cycles on biological clock detected by wheel running under intermediate light intensity (~50 lux). I advanced LD cycles by 8 hrs transiently for 1, 2, 3 or 4 day(s) and turned off the light. Representative double-plotted actograms of WT (upper) and *V1a*$^{-/-}$*V1b*$^{-/-}$ (lower), activity onset (means ± SEM), and amounts of phase advance values (means ± SEM) are shown as indicated in the figure (n = 10-13 for both genotypes; **$P < 0.01$, ***$P < 0.001$, unpaired t test). Note that one-day phase advance in LD cycle induced almost 8-hr advance in *V1a*$^{-/-}$*V1b*$^{-/-}$ mice behavior. Black and red colors indicate WT and *V1a*$^{-/-}$*V1b*$^{-/-}$, respectively. Top bars indicate the initial LD cycle.

Moreover, there were no significant differences between genotypes in the phase delay in locomotor activities, the level of *Per1* induction, or the number of *Per1*-positive cells induced by a light pulse at CT14 (CT represents circadian time; CT0 is subjective dawn and CT12 is subjective dusk) (Fig. 13), which suggested that the light response of *V1a*$^{-/-}$*V1b*$^{-/-}$ SCN clock is similar to that of WT.

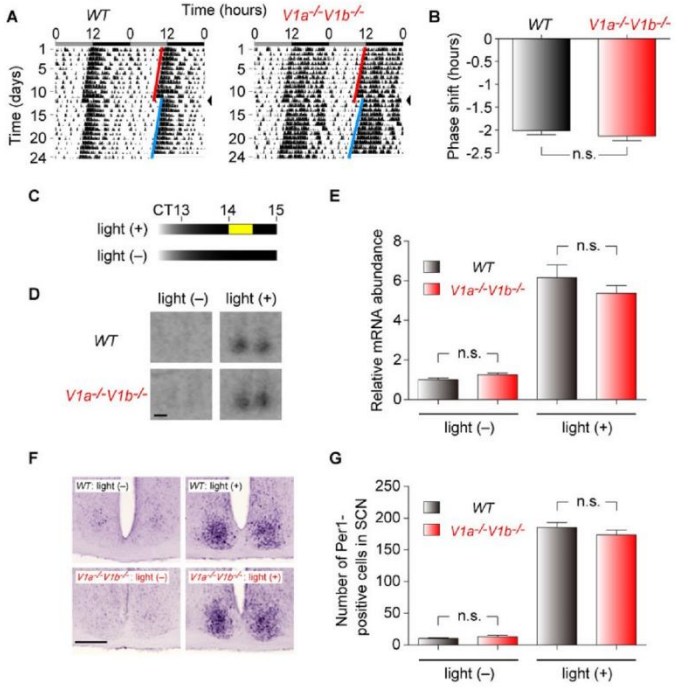

Fig. 13. Effect of a light pulse on locomotor behavior and *Per1* induction in the SCN. Mice were illuminated with an intermediate intensity light (~50 lux) for 30 mins at CT14. (A) Representative double-plotted actograms of WT (left) and *V1a*$^{-/-}$*V1b*$^{-/-}$ (right). (B) Quantification of the magnitude of phase shifts by a resetting light exposure (30 mins of ~50 lux light at CT14, n = 10 for both genotypes). By convention, delays are negative. Note that WT and *V1a*$^{-/-}$*V1b*$^{-/-}$ mice have virtually the same phase shift magnitude. (C) Mice were sacrificed at CT15 with or without a light exposure (30 mins of ~50 lux light at CT14). (D) Representative autoradiographs of radioisotopic *in situ* hybridization showing *Per1* expression in WT and *V1a*$^{-/-}$*V1b*$^{-/-}$ SCN. Bar, 200 μm. (E) Relative *Per1* mRNA abundance quantified with radioisotopic *in situ* hybridization. Values are plotted as means ± SEM (n = 3-4, the value in WT SCN without light stimulation was adjusted to 1). (F) Representative photomicrographs of digoxigenin *in situ* hybridization showing *Per1* expression in WT and *V1a*$^{-/-}$*V1b*$^{-/-}$ SCN. Bar, 200 μm. Note that light stimulation induced *Per1* mRNA in the ventrolateral region in both genotypes. (G) The number of *Per1*-positive cells in the SCN. Values are the sum of 3 sections of each SCN and plotted as means ± SEM (n = 4-6). An observer blind to the experimental condition counted the number of positive cells in the SCN. Black and red colors indicate WT and *V1a*$^{-/-}$*V1b*$^{-/-}$, respectively.

Oscillations of clock genes during jet lag.

To characterize molecular changes in the SCN during jet lag, I examined clock gene expression in laser-microdissected SCN samples collected from mice killed every 4 hrs (Fig. 14).

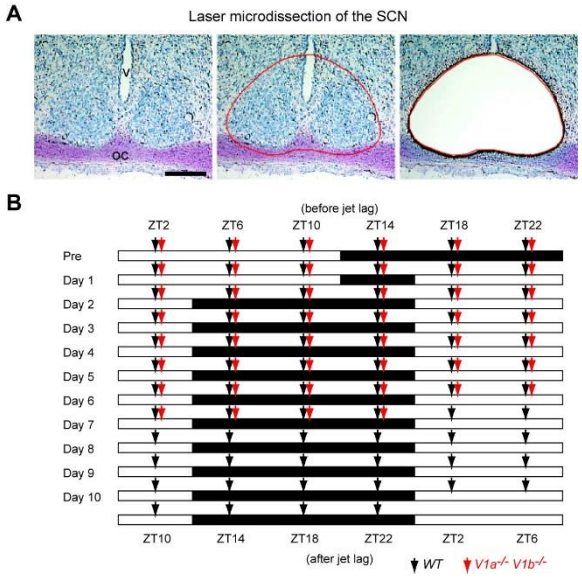

Fig. 14. Laser microdissection of the SCN and sampling time schedule. (A) The micrographs show a representative tissue section stained with toluidine blue before and after laser microdissection. Note the dense accumulation of stained cells in the SCN. Red line delineates the laser-track. v, third ventricle; oc, optic chiasm. Bar, 200 μm. (B) Two mice were sacrificed every 4 hrs before (40 hrs) and after phase advance in LD cycles until 10 days for WT (70 sampling points: black arrows, total 140 mice) and 6 days for *V1a*$^{-/-}$*V1b*$^{-/-}$ mice (46 sampling points: red arrows, total 92 mice), respectively.

Before a phase advance in LD cycles, all transcripts examined in both genotypes showed a similar expression pattern: *Per1*, *Per2*, and *Dbp* showed comparable peak values around the middle of the day, ZT6 to ZT10 (ZT represents Zeitgeber time used in LD cycle; ZT0 is lights on and ZT12 is lights-off), whereas *Bmal1* was highest around ZT14 (Fig. 15). In contrast, after a phase advance in LD cycles, there were striking differences between genotypes in clock gene expression. In WT mice, *Per1* and *Per2* expression lost rhythmicity on days 1 to 2, oscillated with very low amplitude on days 3 to 7, and recovered to the original circadian expression pattern on day 8. *Bmal1* and *Dbp* expression also required 8 to 9 days for complete recovery to the original circadian expression pattern, with severely perturbed rhythmicity on days 1 to 5 (Fig. 15). In *V1a*$^{-/-}$*V1b*$^{-/-}$ mice, although the expression of some genes was partially perturbed on days 1 to 2, the peak time and amplitude in oscillations of all four clock genes recovered on day 3 (Fig. 15).

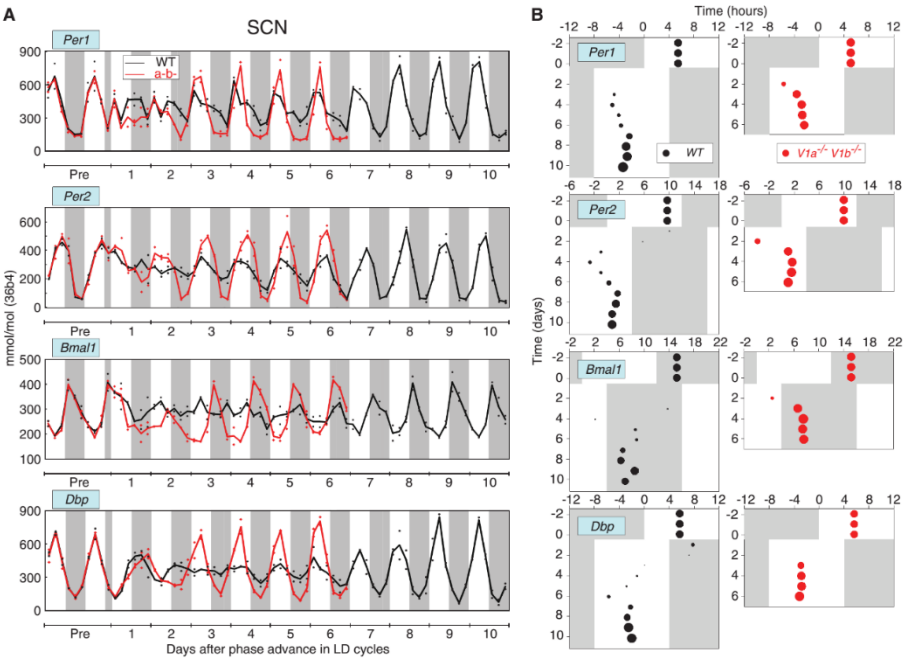

Fig. 15. *V1a*$^{-/-}$*V1b*$^{-/-}$ mice subjected to an experimental jet-lag paradigm show fast reentrainment of SCN clock gene rhythms. (A) Measurement by qRT-PCR of clock gene expression profiles (*Per1*, *Per2*, *Bmal1*, and *Dbp*) in the laser microdissected SCN (Fig. 14A), obtained every 4 hrs continuously throughout the jet-lag schedule (Fig. 14B). LD cycles were advanced by 8 hrs on day 1. Graph indicates an average of two mice independently collected and measured. Note that all transcripts examined in WT SCN lost rhythmicity right after jet lag. (B) Peak time- and amplitude-based kinetic analyses of reentrainment in clock gene expression rhythms. Peak time and amplitude are shown schematically as dots, position and diameter representing peak time and daily amplitude, respectively. Dots were omitted when daily peak time was ambiguous. Dots before an 8-hr phase advance are triple-plotted for better visualization. Black and red colors indicate WT and *V1a*$^{-/-}$*V1b*$^{-/-}$, respectively.

Consistent with these results, cellular level analysis by digoxigenin *in situ* hybridization revealed that the robust oscillation in *Per1* and *Dbp* in WT SCN was severely perturbed on day 3 after a phase advance in LD cycles, but not in *V1a*$^{-/-}$*V1b*$^{-/-}$ SCN (Fig. 16).

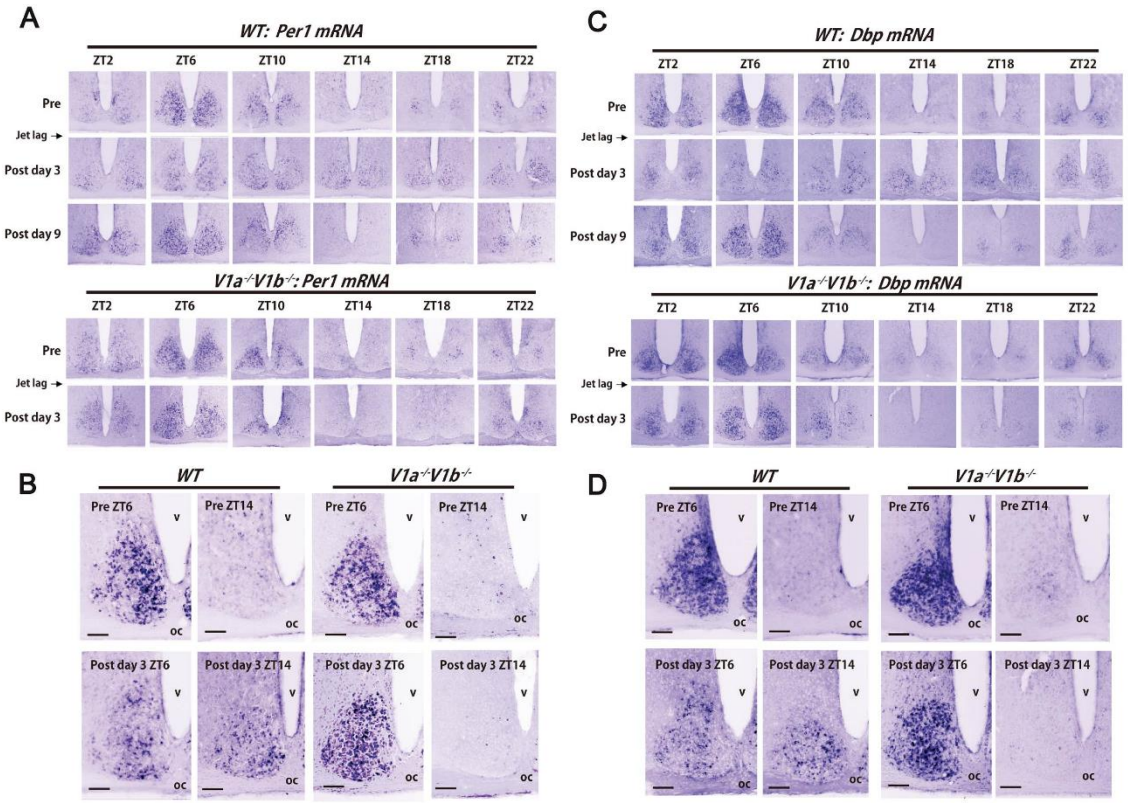

Fig. 16. Digoxigenin *in situ* hybridization showing expression of *Per1* (A and B) and *Dbp* (C and D) in the SCN under experimental jet-lag paradigm. WT and *V1a*$^{-/-}$*V1b*$^{-/-}$ mice were sampled every 4 hrs before and at day 3 and 9 after 8-hr phase advance in LD cycles. (A and C) Low power micrographs. (B and D) High power micrographs. Before jet lag, *Per1* and *Dbp* expressions began to increase at ZT2 from the periventricular part of the dorsomedial SCN, spread widely all over the SCN at ZT6, began to decrease in all SCN regions at ZT10, and were identified in a few SCN cells during ZT14-22. No genotype difference was noted in the topographical distribution in *Per1* and *Dbp* expressions before jet lag. During jet lag, dramatic differences between genotypes were found in both *Per1* and *Dbp* expressions. *Per1* and *Dbp* expressions scattered in WT SCN around the clock without rhythmicity at day 3, and rhythmic expressions in *Per1* and *Dbp* recovered at day 9. In contrast, topographical circadian expressions of *Per1* and *Dbp* in *V1a*$^{-/-}$*V1b*$^{-/-}$ SCN were observed at day 3. oc, optic chiasm; v, third ventricle. Bar, 100 μm. The results shown are representative of three independent experiments that yielded similar results.

I next examined the phase-transition kinetics of clock gene rhythms in peripheral organs and monitored temperature rhythms. In contrast to what I observed with the SCN, clock gene rhythm amplitudes in the liver were maintained during reentrainment. However, the peak time was severely affected after a phase advance in LD cycles: phase recovery required 9 to 10 days in WT mice but only 5 days in *V1a*$^{-/-}$*V1b*$^{-/-}$ mice (Fig. 17). Similar reentrainment kinetics was also observed in the kidney (Fig. 18).

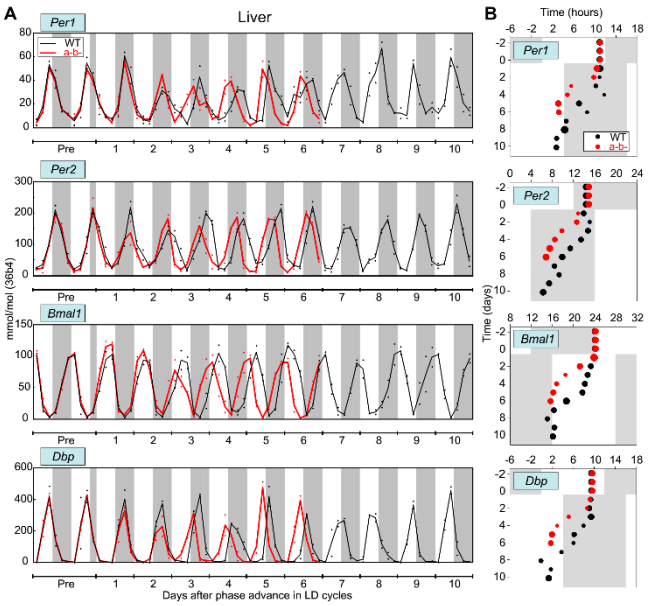

Fig. 17. *V1a*$^{-/-}$*V1b*$^{-/-}$ mice subjected to an experimental jet-lag paradigm show faster reentrainment of clock genes in liver tissue. (A) Measurement by qRT-PCR of clock gene expression profiles (*Per1*, *Per2*, *Bmal1*, and *Dbp*) in the liver of WT and *V1a*$^{-/-}$*V1b*$^{-/-}$ mice before and after an 8-hr phase advance in LD cycles. Graph indicates an average of two mice independently collected and measured. (B) Peak time- and amplitude-based kinetic analyses of reentrainment in the liver of WT and *V1a*$^{-/-}$*V1b*$^{-/-}$ mice (see legend of Fig. 15). Black and red colors indicate WT and *V1a*$^{-/-}$*V1b*$^{-/-}$, respectively.

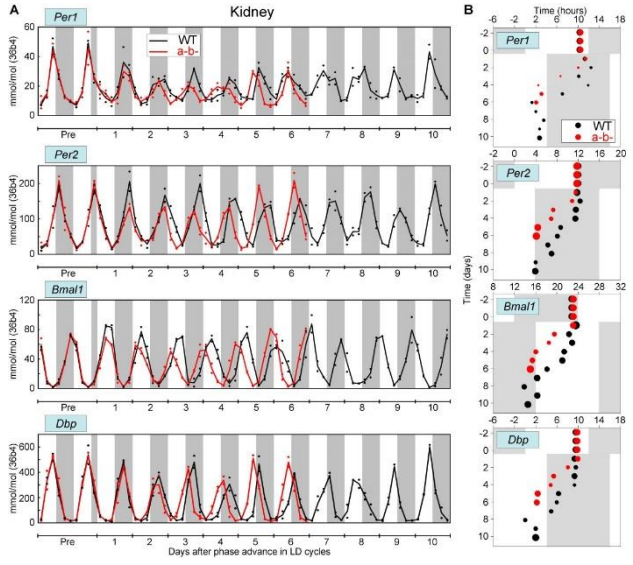

Fig. 18. qRT-PCR-based measurement of clock gene expression profiles in the kidney under jet lag paradigm. (A) Graph indicates an average of 2 mice independently collected and measured. (B) Peak time- and amplitude-based kinetic analysis of reentrainment in the kidney of WT and *V1a*$^{-/-}$*V1b*$^{-/-}$ mice (see legend in Fig. 15 for details). Black and red colors indicate WT and *V1a*$^{-/-}$*V1b*$^{-/-}$, respectively.

Body temperature rhythms peaking at ZT16 reentrained within 5 days in *V1a*$^{-/-}$*V1b*$^{-/-}$ mice, but needed 10 days in WT mice after a phase advance in LD cycles (Fig. 19).

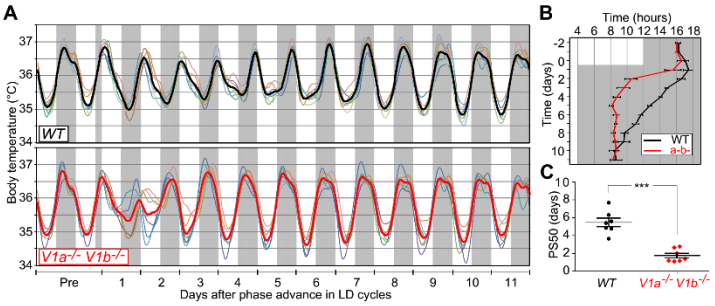

Fig. 19. *V1a*$^{-/-}$*V1b*$^{-/-}$ mice subjected to an experimental jet-lag paradigm show faster reentrainment of body temperature rhythms. (A) Continuous monitoring of body temperature by a thermometer inserted into the peritoneum every 20 mins before and after an 8-hr phase advance in LD cycles. Thin and thick waves indicate the body temperature rhythms of individual mouse and mean of each genotype, respectively (n = 7, both genotypes). (B and C) Daily peak time of body temperature rhythms (B), and PS50 values of peak time transitions (C) [means ± SEM; n = 7 (both genotypes); ***P < 0.001, unpaired t test)]. Black and red colors indicate WT and *V1a*$^{-/-}$*V1b*$^{-/-}$, respectively.

These results demonstrate the rapid reentrainment of clock gene and body temperature rhythms in *V1a*$^{-/-}$*V1b*$^{-/-}$ mice (see Discussion for comparison with previous jet-lag studies in WT mice). In addition, reestablishment of the central SCN clock occurred 1 to 2 days earlier than that of the peripheral clock or body temperature rhythms in both genotypes, which suggests that the SCN clock determines the recovery period of the whole body.

Vasopressin signaling and interneuronal communication in the SCN.

It is well established that AVP neurons constitute the main population of the SCN and that AVP synthesis and release from the SCN to the cerebrospinal fluid exhibit a robust circadian rhythm (Schwartz and Reppert 1985; Jin et al. 1999). AVP neurons mutually connect via synaptic contacts and form a local circuit within the SCN (Castel et al. 1990). *V1a* and *V1b* are expressed in SCN neurons (Kalamatianos et al. 2004a), and my double *in situ* hybridization results revealed that most AVP neurons also expressed *V1a* in the dorsomedial SCN (Fig. 20), which indicated abundant interactions between AVP neurons. Moreover, transcripts of *AVP* and *V1a* showed robust antiphasic rhythms (Fig. 20), which suggested dynamic circadian regulation of ligand-receptor interactions (Maywood et al. 2011).

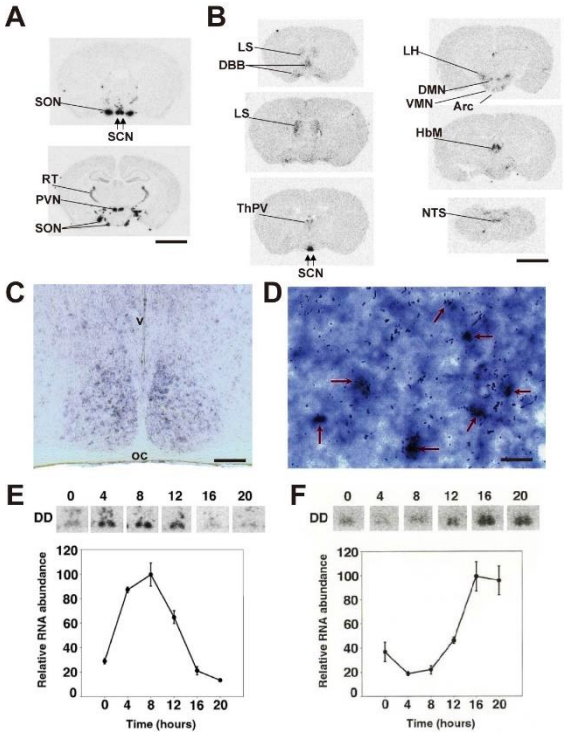

Fig. 20. *In situ* hybridization showing *AVP* and *V1a* expressions in the mouse SCN. (A and B) Autoradiographs showing *AVP* (A) or *V1a* (B) mRNA distributions in the mouse brain. (C and D) Low power (C) and high power (D) photomicrographs of the SCN double *in situ* hybridization with digoxigenin-labelled probe for *V1a* (blue) and isotope-labelled probe for *AVP* (silver grains). Red arrows indicate representative double-labelled cells. (E and F) Circadian expressions of *AVP* (E) and *V1a* (F) in the SCN in DD. Relative RNA abundance was quantified with radioisotopic *in situ* hybridization. Values are plotted as means ± SEM (n = 5) with the peak value adjusted to 100. Representative autoradiographs at the indicated time points are shown on the top. Bar represents 2 mm in A and B, 100 µm in C, 10 µm in D. Abbreviations: Arc, hypothalamic arcuate nucleus; DBB, nucleus of the diagonal band of Broca; DMN, hypothalamic dorsomedial nucleus; HbM, medial habenular nucleus; LS, lateral septal nucleus; oc, optic chiasm; LH, lateral hypothalamus; NTS, nucleus tractus solitarius; PVN, hypothalamic paraventricular nucleus; RT, reticular thalamic nucleus; SCN, suprachiasmatic nucleus; SON, supraoptic nucleus; ThPV, paraventricular thalamic nucleus; v, third ventricle; VMN ventromedial nucleus.

I hypothesized that the disruption of clock gene rhythms observed in WT SCN, but not in *V1a*$^{-/-}$*V1b*$^{-/-}$ SCN, during jet lag might be due to alterations in AVP-mediated interneuronal communication in the SCN. To investigate the effect of AVP-mediated communication on cellular rhythms, I performed real-time bioluminescence imaging of SCN slices from WT and *V1a*$^{-/-}$*V1b*$^{-/-}$ mice carrying *Per1*-promoter–luciferase (*Per1-luc*), which allows simultaneous measurement of hundreds of cellular rhythms (Yamaguchi et al. 2003). Bioluminescence emitted from WT or *V1a*$^{-/-}$*V1b*$^{-/-}$ SCN showed robust rhythms, which was perturbed by administration of cycloheximide (CHX, Fig. 21A). After CHX withdrawal, the amplitudes of bioluminescence rhythms in WT SCN recovered quickly, while those in *V1a*$^{-/-}$*V1b*$^{-/-}$ SCN were relatively small with lower peak and higher trough

levels. Both WT and *V1a*$^{-/-}$*V1b*$^{-/-}$ SCN neurons showed robust rhythms in a spatiotemporally organized manner, starting from the dorsomedial portion and spreading to the ventrolateral side. Among WT SCN neurons, such a phase order was observed even after CHX treatment; very few cells showed faint bioluminescence at 0 hr when total SCN bioluminescence was trough, cells in the dorsomedial part showed strong bioluminescence at 4 hr, bioluminescence was widely observed throughout the SCN at 10 hr and started to descend later, and finally almost all the cells did not show substantial level of bioluminescence (Fig. 21, B and C). On the other hand, the phase order among *V1a*$^{-/-}$*V1b*$^{-/-}$ SCN neurons was severely permuted: many cells showed strong bioluminescence not only at 10 hr, but also at 0 hr (Fig. 21, B and C). The permuted phase order in *V1a*$^{-/-}$*V1b*$^{-/-}$ SCN neurons after CHX treatment is consistent with the small amplitude of total *V1a*$^{-/-}$*V1b*$^{-/-}$ SCN bioluminescence in which antiphasic unit oscillations would cancel each other and result in a dull oscillation as a whole. These results indicate that *V1a*$^{-/-}$*V1b*$^{-/-}$ SCN is more amenable to perturbation than WT SCN. Conceivably, it is this vulnerability in interneuronal coupling that enables the mutant SCN to reentrain to altered lighting schedules more rapidly.

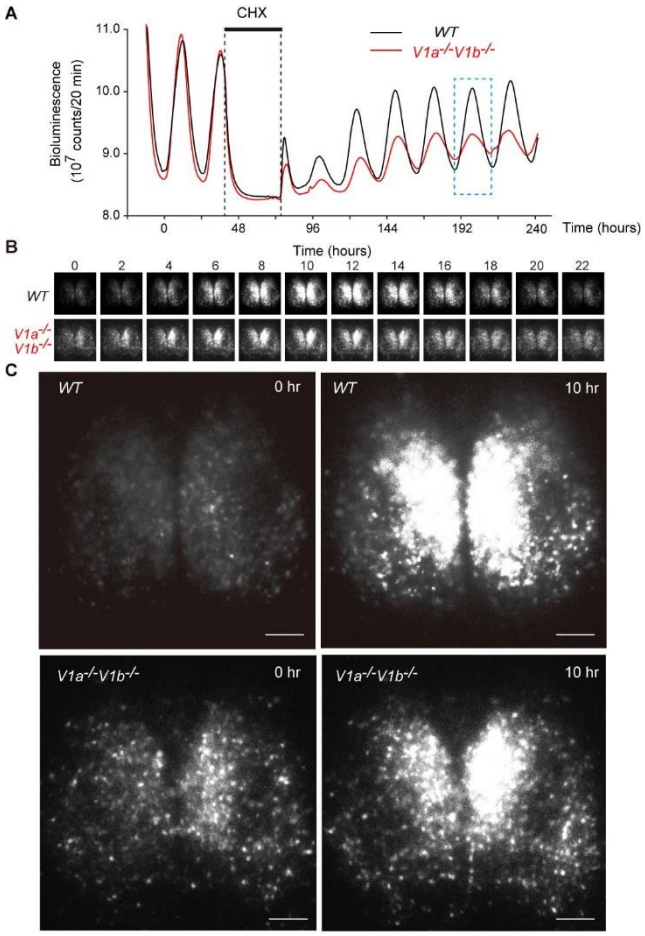

Fig. 21. Permuted phase order in *V1a*$^{-/-}$*V1b*$^{-/-}$ SCN after resetting cellular clocks with cycloheximide. Temporal changes in bioluminescence signals were examined in SCN slice culture from WT and *V1a*$^{-/-}$*V1b*$^{-/-}$ mice carrying *Per1-luc* reporter. (A) Total SCN bioluminescence in both genotypes before and after treatment with CHX (10 µg/ml for 36 hrs). Note the difference in recovery of amplitudes between WT and *V1a*$^{-/-}$*V1b*$^{-/-}$ SCN after CHX washout. (B) Two-hourly images of the SCN slice from WT and *V1a*$^{-/-}$*V1b*$^{-/-}$ mice during sixth cycle after CHX washout (indicated with a blue dashed rectangle in panel A). The trough time of total SCN bioluminescence was set to time 0. (C) High power photomicrographs of the SCN at a trough time (0 hr) and a peak time (10 hr) of total SCN bioluminescence. Note that cells high in bioluminescence were observed in wider area of *V1a*$^{-/-}$*V1b*$^{-/-}$ SCN at both times. Bars, 100 µm.

Pharmacological inhibition of V1a/V1b signaling.

To evaluate the effect of AVP-mediated cellular interaction in WT SCN under jet-lag conditions, I transiently blocked V1a and V1b signaling in the SCN of adult WT mice *in vivo* during jet lag. I applied a mixture of OPC-21268 (V1a antagonist) and SSR 149415 (V1b antagonist) just over the SCN through an osmotic minipump (Doi et al. 2011). Mice receiving this treatment reentrained significantly faster to new LD cycles in a dose-dependent manner (Fig. 22).

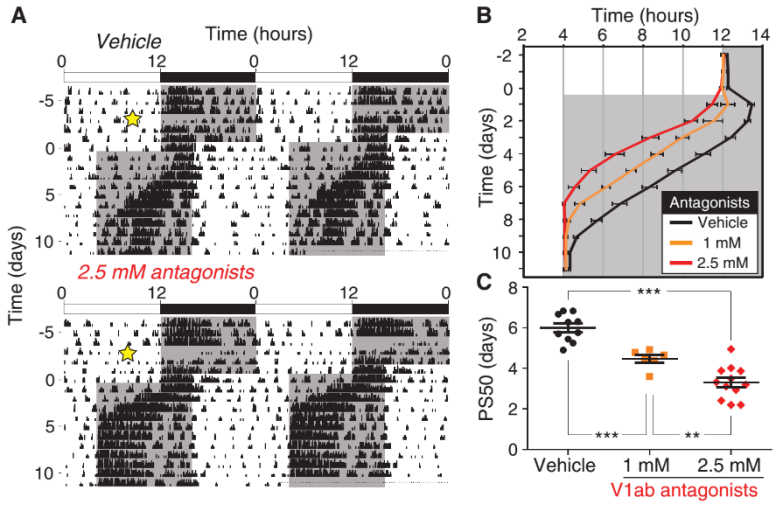

Fig. 22. Direct infusion of V1a and V1b antagonists into the SCN enhances the speed of reentrainment of WT mice subjected to an experimental jet-lag paradigm. (A to C) A mixture of OPC-21268 (V1a antagonist) and SSR 149415 (V1b antagonist) was applied over the SCN by osmotic minipump, and LD cycles were advanced by 8 hrs on day 1. Two concentrations of each antagonist (1 mM or 2.5 mM) were applied. (A) Representative double-plotted actograms of vehicle- (top) or 2.5 mM antagonist-treated mice (bottom). Time of surgery is indicated by a yellow star. (B) Activity onset [means ± SEM; n = 10, 6, and 12 in vehicle, 1 mM, and 2.5 mM groups, respectively). (C) PS50 values of onset time transitions (means ± SEM). One-way analysis of variance (ANOVA), F(2, 25) = 39.09; $P < 0.0001$. Tukey-Kramer post hoc test was performed for comparison among the groups. $^{**}P < 0.01$, $^{***}P < 0.001$.

These results support the crucial role of V1a and V1b signaling in the SCN in determining the speed of reentrainment after a phase advance in LD cycles and exclude the possibility that rapid reentrainment in *V1a*$^{-/-}$*V1b*$^{-/-}$ mice is simply caused by a developmental failure in mutant mice.

Discussion

The cause of jet lag syndrome after transmeridian flights has been explained as arising from desynchronization between the internal clock and external time. However, the identification of clock genes (Tei et al. 1997; Sun et al. 1997; King et al. 1997) has provided a strong base for new investigations into the mechanisms of jet lag syndrome at the molecular, cellular, and systemic levels. A pioneering work employed *ex vivo* cultured slices of the SCN and other tissues from *Per1-luc* transgenic rats, and reported that *Per1* oscillations in SCN slices reentrained in only a few days after jet lag, but those in peripheral organs required 1 week for reentrainment (Yamazaki et al. 2000). Essentially the same results were recently reproduced using SCN slices from mPer2^{LUC} knock-in mice (Davidson et al. 2009). These results were confirmed *in vivo* by analyzing daily expression of *Per1* and *Per2* genes during jet lag by semiquantitative *in situ* hybridization (Kiessling et al. 2010). Interestingly, this *in vivo* study also reported that *Per* genes reentrained more quickly than other clock genes, which is consistent with another *in situ* hybridization analysis in the SCN *in vivo* (Reddy et al. 2002). These observations were based on analysis of the daily peak time transition of each clock gene during jet lag; however, determination of the circadian *Per* expression peak time solely from its daily expression pattern would be very difficult compared with other genes. *Per* genes are not only circadian oscillatory genes but are also light-inducible immediate early genes (Shigeyoshi et al. 1997), unlike other clock genes such as *Cry1* and *Dbp*, which are not light-inducible (Okamura et al. 1999, Mitsui et al. 2001). Thus, it is quite difficult to determine whether rhythmic *Per* expression across a day indicates its circadian oscillation or simple induction by light.

The outstanding feature of clock gene oscillations in the SCN is their robustness with high amplitude, which was not taken into account in previous studies due to methodological limitations. To address this issue, I performed consecutive sampling of the SCN obtained precisely with laser microdissection, and measured expression of each clock gene by quantitative RT-PCR. The sample size in this study reached 6 time points per day over 11 days, much larger than previous sampling resolutions (e.g. discontinuous sampling at day 1, 3, and 8 after jet lag (Reddy et al. 2002). This sampling resolution enabled me to calculate and compare the amplitude and phase of each clock gene oscillation throughout the jet lag period. In this study, the amplitude of *Pers* as well as *Bmal1* and *Dbp*, which all showed robust oscillations before jet lag, were profoundly damped during jet lag. *Per* genes showed slightly higher expression in the morning than at other time points during jet lag. Since these weak and unstable peaks always appeared

immediately after the light was turned on, it was extremely difficult to judge whether these peaks were true circadian peaks or merely the result of light-induced expression. Thus, I evaluated both the amplitude and phase to determine reentrainment of clock gene oscillations. According to this analysis and in contrast to previous reports, *Per* genes do not significantly reentrain faster than other genes, and I conclude that all clock genes reentrain virtually at the same time.

In summary, I have shown that mice lacking the vasopressin V1a and V1b receptors are resistant to jet lag, as measured by locomotor activity, clock gene expressions, and body temperature. The mutant mice rapidly phase-shift to a new environmental LD cycle. Like AVP and its receptors, vasoactive intestinal polypeptide and its receptor VPAC2 are also expressed in the SCN and have been linked to the circadian clock. However, deficiency of VPAC2 in mice has severe consequences on behavior and neural activity rhythms, as well as clock gene oscillations (Aton et al. 2005; Harmar et al. 2002). In contrast, I showed that the absence of V1a and V1b receptors does not elicit overt anomalies in behavioral and clock gene expression rhythms under regular LD and constant DD conditions. Previous studies suggested that genetic manipulation of AVP or its receptor have only minor effects on circadian behavior (Li et al. 2009; Groblewski et al. 1981). However, I here demonstrated that rhythms of behavior, clock gene oscillation, and body temperature in $V1a^{-/-}V1b^{-/-}$ mice reentrain immediately after a phase advance in LD cycles. I hypothesize that this rapid reentrainment occurs because AVP-mediated interneuronal communication, which confers on the SCN an intrinsic resistance to external perturbations like jet lag, is missing in $V1a^{-/-}V1b^{-/-}$ mice.

Epidemiological studies have shown that chronic jet lag and rotating shift work can increase an individual's risk of developing hypertension, obesity, and other metabolic disorders. The present study identified vasopressin signaling as a possible therapeutic target for the management of circadian rhythm misalignment.

Chapter 2

Behavioral difference in mice after two ways of jet lag: light-phase advance and dark-phase advance

In nature, multiple environmental factors oscillate over the daily cycles. Among them, the most important timing cue for human beings to entrain is the 24-hr solar cycles of light and darkness. Thus, jet lag is caused mainly by improper timing of the body clock in a new time zone and causes us a variety of symptoms such as poor sleep during the new nighttime, poor performance during the new daytime, and gastrointestinal disturbances (Waterhouse et al. 2007).

For photic entrainment to occur, the response of the internal clock to light is different between the subjective night and the subjective day. Light generally does not shift the phase of the circadian rhythm when presented during the subjective day, while light pulse stimuli reset the phase of clock oscillation during the subjective night. Light early and late in the subjective nighttime produces phase delays and advances of a circadian rhythm, respectively. The endogenous circadian clock synchronizes with the external LD cycles through the resetting mechanism (Moore-Ede et al. 1982).

Experimentally, there are two ways of phase advances in LD cycles. In one condition, new LD cycles abruptly start at ZT16, which is in dark phase before jet lag (abrupt light condition, ALC). In the other condition, new LD cycles abruptly start at ZT4, which is in light phase before jet lag (abrupt dark condition, ADC). In this chapter, I examined the effect of two types of jet lag, ALC and ADC, on the phase shifts of locomotor activities, and found that there was a significant difference in the amounts of the phase shifts of locomotor activities between two ways of jet lag. Since the suprachiasmatic nucleus is the master clock of the circadian rhythms, the role of the nucleus determining the phase after jet lag should be examined in future studies.

Materials and Methods

Mouse and behavioral activity monitoring for jet lag experiments.

V1a$^{-/-}$ and *V1b*$^{-/-}$ mice (Koshimizu et al. 2006; Tanoue et al. 2004) were backcrossed to the C57Bl/6 background, and were mated to generate *V1a*$^{-/-}$*V1b*$^{-/-}$ double knockout mice. *V1a*$^{-/-}$*V1b*$^{-/-}$ and wild-type C57Bl/6 mice (male, 2-5 months old, age-matched between genotypes) were housed individually in light-tight, ventilated closets within a temperature- and humidity-controlled facility with *ad libitum* access to food and water. The animals were entrained on a 12-hr-light (~200 lux fluorescent light)/12-hr-dark cycle at least two weeks to synchronize (entrain) the circadian clock of the mice to the ambient light-dark cycle, and then light-dark cycles were 8-hr phase-advanced or phase-delayed. Where indicated, a light emitting diode light bulb (~50 lux) was also used as an intermediate light intensity. Locomotor activity was recorded in 5-min bins with passive (pyroelectric) infrared sensor (FA-05 F5B; Omron) or wheel running, and the data obtained were analysed with Clocklab software (Actimetrics) developed on MatLab (Mathworks). Free-running period was determined with a linear regression line fit to the activity onsets, based on animal behaviors in a 14-day interval taken 3 days after the start of DD condition. The amounts of phase advance or phase delay in behavioral activity after release to DD were determined as the time difference between regression lines of activity onsets before and after the start of DD. For the pulse-induced shift experiments, mice put in DD were exposed to a 30 min light pulse at either CT2, CT6, CT10, CT14, CT18, or CT22. Phase shifts were quantified as the time difference before and after the light application. All experiments were conducted in accordance with the ethical guidelines of the Kyoto University Animal Research Committee.

Laser microdissection of the SCN.

Mice were killed by cervical dislocation, and the eyes were removed under a safety red light when sampled in dark condition. The brain was then isolated from the skull under room light and was frozen immediately on dry ice. Coronal brain section (30 μm thick) containing the SCN was prepared using a cryostat microtome (CM3050S, Leica) and mounted on POL-membrane slides (Leica). Sections were fixed for 3 mins in an ice-cold mixture of ethanol and acetic acid (19:1), rinsed briefly in ice-cold water, stained for 30 secs in ice-cold water containing 0.05% toluidine blue, followed by two brief washes in ice-cold water (all the solutions were RNase-free). After wiping off excess water, slides were quickly air dried at room temperature. As soon as moistures in the sections decreased enough for laser-cutting, cells in the SCN were microdissected using a LMD7000 device

(Leica; 10× magnification) and lysed in Trizol reagent (Thermo Fisher Scientific), and total RNA was purified using the RNeasy micro kit (Qiagen).

Quantitative RT-PCR.

Total RNA in the SCN and liver was converted to cDNA using SuperScript VILO cDNA Synthesis Kit (Thermo Fisher Scientific). Quantitative PCR analysis of the individual cDNAs was performed as described previously (Doi *et al.*, 2010). Absolute quantification of each gene level was achieved by comparison of the cloned plasmid DNA as a standard, and results were normalized to *36b4* mRNA levels. The primer sets used were following: *36b4* (NM_007475), Fw: 5'-ctc act gag att cgg gat atg-3', Rv: 5'-ctc cca cct tgt ctc cag tc-3'; *Per1* (NM_011065), Fw: 5'-tgg ctc aag tgg caa tga gtc-3', Rv: 5'-ggc tcg agc tga ctg ttc act-3'; *Per2* (NM_011066), Fw: 5'-cca tcc aca aga aga tcc tac-3', Rv: 5'-gct cca cgg gtt gat gaa gc-3'; *Bmal1* (NM_007489), Fw: 5'-cct aat tct cag ggc agc aga t-3', Rv: 5'-tcc agt ctt ggc atc aat gag t-3'; *Dbp* (NM_016974), Fw: 5'-aat gac ctt tga acc tga tcc cgc t-3', Rv: 5'-gct cca gta ctt ctc atc ctt ctg t-3'; *cFos* (NM_010234), Fw: 5'-aga gcg gga atg gtg aag ac-3', Rv: 5'-ggt ggg ctg cca aaa taa ac-3'. Melt curve analysis was performed to confirm each of the final PCR product.

Measurement of body temperature rhythm.

Core body temperature was continuously recorded every 20 mins in WT or *V1a*$^{-/-}$*V1b*$^{-/-}$ mice at 8 weeks of age using Thermochron iButton DS1291H (Maxim, San Jose) inserted into the peritoneal cavity. Following 2 weeks in 12L:12D condition for recovery, LD cycles were advanced by 8 hrs. After 2 weeks, the animals were killed and the temperature data were retrieved from the iButtons. Since the body temperature in mice highly fluctuated throughout the day, the moving average with 4-hr window size was applied three times to the original data to obtain the peak time and evaluate the phase of body temperature rhythm.

V1a and V1b antagonists infusion over the SCN.

For pharmacological inhibition of V1a and V1b signaling, a mixture of OPC-21268 (Sigma-Aldrich), a V1a antagonist, and SSR 149415 (Axon Medchem), a V1b antagonist, was continuously delivered to the SCN via an osmotic pump as described previously (Doi *et al.*, 2011). Then, animals were returned to their home cages and LD cycles were advanced by 8 hrs at 3-5 days after the surgery.

***Per1-luc* SCN slice culture.**

Per1-luc SCN slice culture and bioluminescence recording were performed as described previously (Doi *et al.*, 2011). *Per1-luc-V1a*$^{-/-}$*V1b*$^{-/-}$ mice were generated by crossing *Per1-luc* transgenic mice and *V1a*$^{-/-}$*V1b*$^{-/-}$ mice. At 3 hr after the second peak of total SCN bioluminescence, SCN slice was moved to the medium containing 10 μg/ml of CHX and kept for 36 hrs. Then, SCN slices were washed with fresh medium and luminescence of the slices was recorded for more than 7 days.

Radioisotopic *in situ* hybridization.

In situ hybridization analysis was performed as described (Shigeyoshi *et al.*, 1997) with the following gene-specific probes: for *Per1*, the antisense probe covering nucleotides 812-1651 of the *Per1* mRNA (Genbank, NM_011065); for *AVP*, nucleotides 378-575 (NM_016992.2); for *V1a*, nucleotides 227-1786 (NM_016847.2). Briefly, paraformaldehyde-fixed brains were frozen and sectioned at a thickness of 30 μm. Then, the free-floating tissue sections were transferred through 2 x SSC, proteinase K (1 μg/ml, 0.1 M Tris buffer [pH 8.0]; 50 mM EDTA) for 10 mins at 37°C, 0.25% acetic anhydride in 0.1 M triethanolamine for 10 mins, and 2 x SSC for 10 mins. The sections were then incubated in the hybridization buffer [55% formamide, 10% dextran sulfate, 10 mM Tris-HCl (pH 8.0), 1 mM EDTA (pH 8.0), 0.6 M NaCl, 0.2% N-laurylsarcosine, 500 μg/ml tRNA, 1 x Denhardt's, 0.25% SDS, and 10 mM dithiothreitol (DTT)] containing radiolabeled riboprobes for 16 hrs at 60°C. Following a high-stringency posthybridization wash, the sections were treated with RNase A. Air-dried sections were exposed to X-ray films (Kodak Biomax).

Digoxigenin *in situ* hybridization.

In situ hybridization analysis was performed with the following gene-specific probes: for *Per1*, the anti-sense probe covering nucleotides 812-1651 of the *Per1* mRNA (Genbank, NM_011065); for *Dbp*, nucleotides 969-1475 (NM_016974); for *V1a*, nucleotides 227-1786 (NM_016847.2). Since digoxigenin-labeled probes allow a better resolution than isotope probes for analyzing the cellular distribution of mRNAs, I made digoxigenin-labeled antisense cRNA probes using digoxigenin-UTP (Roche Diagnostics) following a standard protocol of cRNA synthesis. Tissue preparation, prehybridization, hybridization, and posthybridization washing were the same as for isotope probe hybridization except that I used 30 μm-thick sections. The sections hybridized with the digoxigenin-labeled probe were processed for immunochemistry with a nucleic acid detection kit (Roche Diagnostics). Signals were visualized in a solution containing

nitroblue tetrazolium salt (0.34 mg/ml) and 5-bromo-4-chloro-3-indolyl phosphate toluidinium salt (0.18 mg/ml) (Roche Diagnostics).

Immunohistochemistry for cFos.

For immunohistochemistry of cFos, animals were anesthetized and circulationally perfused with 20 ml of cold fixative (4% paraformaldehyde in 0.1 M PB). The isolated brains were post-fixed with the same fixative for 12 hrs at 4°C and then transferred to 20% sucrose in 0.1 M PB for cryoprotection. Coronal brain cryosections (30 μm thick) were processed for free-floating immunohistochemistry with rabbit polyclonal antibody specific for cFos (ab-7963; abcam). Briefly, the free-floating sections, pretreated with hydrogen peroxide (1.5%, in 0.1 M PB, for 20 min at 4°C), were blocked with 5% horse serum in 0.1 M PB containing 0.3% Triton X-100 (PBX) for 1 hr at room temperature. Then, the sections were incubated with primary antibody (1:10000 dilution in 0.1 M PBX) for 30 mins at RT and then 4 days at 4°C. After washing with PBX, the sections were incubated with secondary antibody [biotinylated anti-rabbit IgG (Vector Laboratories), 1:1000 dilution in PBX] for 12 hrs at 4°C. The imunoreactivities were visualized according to the standard avidin-biotin immunoperoxidase procedure (Vectorstain Elite ABC kit, Vector Laboratories). The immunostained sections were washed with 50 mM Tris-HCl buffer (pH 7.5) and coverslipped with Entellan after dehydration.

Statistical analysis.

Peak time and amplitude values in qRT-PCR were obtained using hand-made program written in R software. To determine PS50 values, sigmoidal dose-response curve with variable slope, $Y = Bottom + (Top – Bottom)/(1 + 10^{(\log PS50 – X) HillSlope})$, was fitted to the onset/offset time points (locomotor activity) or the peak time points (body temperature) using GraphPad Prism software (Kiessling *et al.*, 2010). I compared the data in behavioral and body temperature experiments between WT and $V1a^{-/-}V1b^{-/-}$ mice with two-tailed unpaired *t* test. For the experiments in which three or more test groups were compared, I used one-way analysis of variance (ANOVA) with Tukey-Kramer post-hoc test. All the statistical comparisons were performed with GraphPad Prism software. A statistically significant difference was assumed with *P* values less than 0.05.

References

An, S. et al., 2012. Spatiotemporal distribution of vasoactive intestinal polypeptide receptor 2 in mouse suprachiasmatic nucleus. *The Journal of comparative neurology*, 520(12), pp.2730–41.

Aronin, N. et al., 1990. Light regulates expression of a Fos-related protein in rat suprachiasmatic nuclei. *Proceedings of the National Academy of Sciences of the United States of America*, 87(15), pp.5959–62.

Aton, S.J. et al., 2005. Vasoactive intestinal polypeptide mediates circadian rhythmicity and synchrony in mammalian clock neurons. *Nature neuroscience*, 8(4), pp.476–83.

Butler, M.P. & Silver, R., 2009. Basis of robustness and resilience in the suprachiasmatic nucleus: individual neurons form nodes in circuits that cycle daily. *Journal of biological rhythms*, 24(5), pp.340–52.

Buxton, O.M. et al., 2012. Adverse metabolic consequences in humans of prolonged sleep restriction combined with circadian disruption. *Science translational medicine*, 4(129), p.129ra43.

Cao, R. et al., 2013. Mitogen- and stress-activated protein kinase 1 modulates photic entrainment of the suprachiasmatic circadian clock. *The European journal of neuroscience*, 37(1), pp.130–40.

Castel, M. et al., 1990. Vasopressinergic innervation of the mouse suprachiasmatic nucleus: an immuno-electron microscopic analysis. *The Journal of comparative neurology*, 298(2), pp.172–87.

Comperatore, C.A. & Krueger, G.P., 1990. Circadian rhythm desynchronosis, jet lag, shift lag, and coping strategies. *Occupational medicine (Philadelphia, Pa.)*, 5(2), pp.323–41.

Daan, S. & Pittendrigh, C.S., 1976. A Functional analysis of circadian pacemakers in nocturnal rodents. II. *Journal of Comparative Physiology*, 106(3), pp.253–266.

Davidson, A.J. et al., 2009. Visualizing jet lag in the mouse suprachiasmatic nucleus and peripheral circadian timing system. *The European journal of neuroscience*, 29(1), pp.171–80.

Doi, M. et al., 2011. Circadian regulation of intracellular G-protein signalling mediates intercellular synchrony and rhythmicity in the suprachiasmatic nucleus. *Nature communications*, 2(may), p.327.

Doi, M. et al., 2010. Salt-sensitive hypertension in circadian clock-deficient Cry-null mice involves dysregulated adrenal Hsd3b6. *Nature medicine*, 16(1), pp.67–74.

Earnest, D.J. et al., 1990. Photic regulation of c-fos expression in neural components governing the entrainment of circadian rhythms. *Experimental neurology*, 109(3), pp.353–61.

Groblewski, T.A., Nunez, A.A. & Gold, R.M., 1981. Circadian rhythms in vasopressin deficient rats. *Brain research bulletin*, 6(2), pp.125–30.

Harmar, A.J. et al., 2002. The VPAC(2) receptor is essential for circadian function in the mouse suprachiasmatic nuclei. *Cell*, 109(4), pp.497–508.

Hastings, M.H., Maywood, E.S. & O'Neill, J.S., 2008. Cellular circadian pacemaking and the role of cytosolic rhythms. *Current biology : CB*, 18(17), pp.R805–R815.

Jin, X. et al., 1999. A molecular mechanism regulating rhythmic output from the suprachiasmatic circadian clock. *Cell*, 96(1), pp.57–68.

Johnson, R.F., Morin, L.P. & Moore, R.Y., 1988. Retinohypothalamic projections in the hamster and rat demonstrated using cholera toxin. *Brain research*, 462(2), pp.301–12.

Kalamatianos, T., Kalló, I. & Coen, C.W., 2004a. Ageing and the diurnal expression of the mRNAs for vasopressin and for the V1a and V1b vasopressin receptors in the suprachiasmatic nucleus of male rats. *Journal of neuroendocrinology*, 16(6), pp.493–501.

Kalamatianos, T. et al., 2004b. Expression of VIP and/or PACAP receptor mRNA in peptide synthesizing cells within the suprachiasmatic nucleus of the rat and in its efferent target sites. *The Journal of comparative neurology*, 475(1), pp.19–35.

Kiessling, S., Eichele, G. & Oster, H., 2010. Adrenal glucocorticoids have a key role in circadian resynchronization in a mouse model of jet lag. *The Journal of clinical investigation*, 120(7), pp.2600–9.

King, D.P. et al., 1997. Positional cloning of the mouse circadian clock gene. *Cell*, 89(4), pp.641–53.

Kornhauser, J.M. et al., 1990. Photic and circadian regulation of c-fos gene expression in the hamster suprachiasmatic nucleus. *Neuron*, 5(2), pp.127–34.

Koshimizu, T. et al., 2006. V1a vasopressin receptors maintain normal blood pressure by regulating circulating blood volume and baroreflex sensitivity. *Proceedings of the National Academy of Sciences of the United States of America*, 103(20), pp.7807–12.

Li, J.-D. et al., 2009. Vasopressin receptor V1a regulates circadian rhythms of locomotor activity and expression of clock-controlled genes in the suprachiasmatic nuclei. *American journal of physiology. Regulatory, integrative and comparative physiology*, 296(3), pp.R824–30.

Liu, A.C., Lewis, W.G. & Kay, S. a, 2007. Mammalian circadian signaling networks and therapeutic targets. *Nature chemical biology*, 3(10), pp.630–9.

Maywood, E.S. et al., 2011. A diversity of paracrine signals sustains molecular circadian cycling in suprachiasmatic nucleus circuits. *Proceedings of the National Academy of Sciences of the United States of America*, 108(34), pp.14306–11.

Mitsui, S. et al., 2001. Antagonistic role of E4BP4 and PAR proteins in the circadian oscillatory mechanism. *Genes & development*, 15(8), pp.995–1006.

Mohawk, J.A. & Takahashi, J.S., 2011. Cell autonomy and synchrony of suprachiasmatic nucleus circadian oscillators. *Trends in neurosciences*, 34(7), pp.349–58.

Moore, R.Y., Speh, J.C. & Leak, R.K., 2002. Suprachiasmatic nucleus organization. *Cell and tissue research*, 309(1), pp.89–98.

Moore-Ede, M.C., Sulzman, F.M. & Fuller, C.A., 1982. *The Clocks That Time Us*, Harvard University Press, Cambridge, MA.

Morin, L.P., 1994. The circadian visual system. *Brain research. Brain research reviews*, 19(1), pp.102–27.

Okamura, H. et al., 1999. Photic induction of mPer1 and mPer2 in cry-deficient mice lacking a biological clock. *Science (New York, N.Y.)*, 286(5449), pp.2531–4.

Okamura, H., 2007. Suprachiasmatic nucleus clock time in the mammalian circadian system. *Cold Spring Harbor symposia on quantitative biology*, 72, pp.551–6.

Van den Pol, A.N. & Tsujimoto, K.L., 1985. Neurotransmitters of the hypothalamic suprachiasmatic nucleus: immunocytochemical analysis of 25 neuronal antigens. *Neuroscience*, 15(4), pp.1049–86.

Rea, M.A., 1989. Light increases Fos-related protein immunoreactivity in the rat suprachiasmatic nuclei. *Brain research bulletin*, 23(6), pp.577–81.

Reddy, A.B. et al., 2002. Differential resynchronisation of circadian clock gene expression within the suprachiasmatic nuclei of mice subjected to experimental jet lag. *The Journal of neuroscience : the official journal of the Society for Neuroscience*, 22(17), pp.7326–30.

Reppert, S.M. & Weaver, D.R., 2002. Coordination of circadian timing in mammals. *Nature*, 418(6901), pp.935–41.

Rusak, B. et al., 1990. Light pulses that shift rhythms induce gene expression in the suprachiasmatic nucleus. *Science (New York, N.Y.)*, 248(4960), pp.1237–40.

Sack, R.L., 2009. The pathophysiology of jet lag. *Travel medicine and infectious disease*, 7(2), pp.102–10.

Scheer, F.A.J.L. et al., 2009. Adverse metabolic and cardiovascular consequences of circadian misalignment. *Proceedings of the National Academy of Sciences of the United States of America*, 106(11), pp.4453–8.

Schwartz, W.J. & Reppert, S.M., 1985. Neural regulation of the circadian vasopressin rhythm in cerebrospinal fluid: a pre-eminent role for the suprachiasmatic nuclei. *The Journal of neuroscience : the official journal of the Society for Neuroscience*, 5(10), pp.2771–8.

Schwartz, W.J. & Zimmerman, P., 1990. Circadian timekeeping in BALB/c and C57BL/6 inbred mouse strains. *The Journal of neuroscience : the official journal of the Society for Neuroscience*, 10(11), pp.3685–94.

Shigeyoshi, Y. et al., 1997. Light-induced resetting of a mammalian circadian clock is associated with rapid induction of the mPer1 transcript. *Cell*, 91(7), pp.1043–53.

Sun, Z.S. et al., 1997. RIGUI, a putative mammalian ortholog of the Drosophila period gene. *Cell*, 90(6), pp.1003–11.

Swaab, D.F., Pool, C.W. & Nijveldt, F., 1975. Immunofluorescence of vasopressin and oxytocin in the rat hypothalamo-neurohypophypopseal system. *Journal of neural transmission*, 36(3-4), pp.195–215.

Tanoue, A. et al., 2004. The vasopressin V1b receptor critically regulates hypothalamic-pituitary-adrenal axis activity under both stress and resting conditions. *The Journal of clinical investigation*, 113(2), pp.302–9.

Tei, H. et al., 1997. Circadian oscillation of a mammalian homologue of the Drosophila period gene. *Nature*, 389(6650), pp.512–6.

Waterhouse, J. et al., 2007. Jet lag: trends and coping strategies. *Lancet*, 369(9567), pp.1117–29.

Yamaguchi, S. et al., 2003. Synchronization of cellular clocks in the suprachiasmatic nucleus. *Science (New York, N.Y.)*, 302(5649), pp.1408–12.

Yamaguchi, Y. et al., 2013. Mice genetically deficient in vasopressin V1a and V1b receptors are resistant to jet lag. *Science (New York, N.Y.)*, 342(6154), pp.85–90.

Yamazaki, S. et al., 2000. Resetting central and peripheral circadian oscillators in transgenic rats. *Science (New York, N.Y.)*, 288(5466), pp.682–5.

Young, W.S., Kovács, K. & Lolait, S.J., 1993. The diurnal rhythm in vasopressin V1a receptor expression in the suprachiasmatic nucleus is not dependent on vasopressin. *Endocrinology*, 133(2), pp.585–90.

Acknowledgments

First of all, I wish to express sincerely utmost gratitude to Professor Hitoshi Okamura for providing me the opportunity to study in his laboratory, great experimental environments, and his direction throughout this study. I am also particularly grateful to Assistant Professor Yoshiaki Yamaguchi for his considerable understanding, continuous support, valuable discussions, and thoughtful guidance during the five years of my doctoral course. I also thank Associate Professor Masao Doi and Lecturer Jean-Michel Fustin for their logical thinking guidance, advice and help.

I also gratefully acknowledge all the members of Okamura's lab for encouraging and inspiring me a lot. I could not accomplish this thesis without their supports.

Finally, I would like to express my deepest gratitude to my family and friends for providing strong support and warm encouragement.

March 2015
Toru Suzuki